2018 3rd International Conference on Advanced Robotics and Mechatronics (ICARM)

Integrating Damping Control with Iterative Learning Control for Fast and Precise Scanning of Nanopositioners: A TITO Design*

Jie Ling, Zhao Feng, Min Ming, Zhao Guo, and Xiaohui Xiao, *Member, IEEE*

***Abstract*— Fixed-structure low-order feedback control is a simple and effective damping approach for piezo nanopositioning thanks to the merits of ease of implementation and low computational complexity. However, the tracking performance of scanning motions for nanopositioners is weaken due to the unexpected phase lag and residual periodic errors caused by feedback control alone. In this paper, a feedback integral resonant control (IRC) integrated with a feedforward PID type iterative learning control (ILC) is proposed for vibration damping and precision scanning simultaneously. For a two-input-two-output (TITO) system with cross coupling around the first resonance, a static decoupling matrix is designed to obtain decoupled dynamics. A standard IRC along with ILC is then applied. The parameters in the composite controller are determined to satisfy the convergence condition based on lifted matrix computation. For evaluations, simulations are conducted to check the effectiveness of the parameters. Compared with feedback IRC alone, experimental results demonstrate the superiority of the composite design with more than 85% improvements in RMS errors for both raster and spiral scanning at 20 and 40 Hz.**

I. Introduction

For atomic force microscope (AFM) scanning motions, speed and precision are the two important performance indicators to obtain clear image formation of the specimen surfaces [1-3]. Piezo-actuated flexure-guided nanopositioners are commonly adopted to produce fine mechanical displacements with high-bandwidth and high-resolution [4], [5]. The main helpful properties of piezo actuators are compact structure, large output force, wear-free, rapid response, and little requirement of maintenance [6], [7]. However, the bad side of a piezo nanopositioner which degrades its positioning performance is three-fold: 1) nonlinearity of hysteresis and creep [8], 2) vibrations caused by lightly damped resonant modes [4], [9], 3) cross coupling effect in multi-axis platform [10], [11]. For fast imaging of AFMs in a relatively small scale, i.e. less than 10% of each axis' motion range, the dynamic effect of nonlinearity can be compensated to some degree under properly designed but not specialized feedback or feedforward control [4], [12], [13]. For this reason, this paper focuses on decoupling around the first resonance region and vibration suppression for a two-input-two-output (TITO) nanopositioner system.

The cross-coupling effect between axes can be considered as a type of unmodeled dynamics. A number of efforts have addressed this issue, which can be roughly divided into two categories: 1) decoupled mechanical design [14], [15], 2) control approaches, such as H_∞ [10], model predictive control [16], adaptive control [17], reference model matching [18], dynamic decoupling matrix [19], etc. Some prototypes [14], [15], or commercial products, like the P-561.3CD from Physik Instrumente used in the authors' previous works [3-5], based on decoupled mechanical design, the coupling effects are negligible for that the amplitude gains at the low frequency region (below the first resonance) of the stage are less than -20 dB. However, for high-speed scanning at the frequency near or around the first resonance, cross-coupling effect turns to be remarkable due to the lightly damped modes, which exist in not only dominating motions from *x*-axis input to *x*-axis output but also parasitic motions from *x*-axis input to *y*-axis output. In a word, vibration is the vital problem to be tackled for the TITO system in both dominating and cross coupling dynamics.

Control approaches with respect to vibration rejection for lightly damped modes of nanopositioners are abundant. Feedforward control strategies, such as input shaping [20], model inversion [21], and iterative learning control [22], [23], are proposed and applied because of the features of noise efficiency, packageability, and low cost. Feedback controllers are still necessary to provide robustness against model uncertainty and external disturbance. For this, some general model-based controllers are developed to damp the vibrational modes, such as, H_∞ control [24], loop-shaping [25], linear matrix inequalities-based control [26]. On top of that, some negative-imaginary (NI) controllers are proposed and attract much attention with the advantages of fixed-structure, low order and the ease of implementation. Typical NI controllers contains positive position feedback (PPF) [27], positive velocity and position feedback (PVPF) [12], integral resonant control (IRC) [28], [29], and so on. Among them, for a system with multi resonant modes, IRC is an effective way to damp all the lightly damped modes simultaneously.

To improve the tracking performance further, some composite strategies that integrate feedforward and feedback controllers are also studied. For examples, a high-gain feedback controller combined with an inversion-based feedforward input shaper is proved significant improvement for creep, hysteresis, and vibration compensation in [30]. A feedback H_∞ controller and a feedforward iterative learning control (ILC) are combined in frequency domain for repetitive scanning motions in [31]. A feedforward filter designed based on coprime factorization cooperated with a feedback H_∞ controller is investigated for high-speed nanopositioning in [32]. A properly defined feedback/feedforward architecture can always achieve multi-objective improvements.

*Resrach supported by Shenzhen Science and Technology Program (Grant JCYJ20170306171514468).

Jie Ling, Zhao Feng, Min Ming, Zhao Guo and Xiaohui Xiao are with the School of Power and Mechanical Engineering at Wuhan University, Wuhan 430072, China.(email: jamesling@whu.edu.cn, fengzhaozhao7@whu.edu.cn, mingmin_whu@whu.edu.cn, guozhao@whu.edu.cn, xhxiao@whu.edu.cn)

The motivation of this work is to preliminary investigate an integrated feedback IRC and feedforward ILC framework for *xy*-plane scanning of nanopositioners by taking the advantages of both the two controllers simultaneously. Before the composite controller design, a static decoupling matrix is calculated for the coupled TITO system at high frequency region. Aiming at vibration damping and precision tracking, the standard IRC consists of an inner integral with a feed-through term for damping and an outer integral for tracking is adopted. A PID type ILC is then integrated into the composite design to decrease the repetitive errors in scanning motions. The advantages of this combination are the simplicity of controller design and the ease of implementation. Our contribution lies in the proposal of this feedback/feedforward framework as well as the parameters' determination procedure according to the monotonic convergence condition.

The rest of this paper is arranged as follows. The identified system model is presented in Section II. Section III describes the design details for the static decoupling matrix. In Section IV, the integrated IRC and ILC is discussed with the parameters' determination presented. Experimental results of raster and spiral scanning at 20 and 40 Hz are shown in Section V. Finally, this paper is concluded in Section VI.

II. System Identification

A. Experimental Setup

The proposed feedback/feedforward framework is implemented on a three-axis piezo-actuated nanopositioning stage (P-561.3CD, Physik Instrumente) as depicted in Fig. 1.

The control input is 0~10 V, which is produced by the data output module in dSPACE MicroLabBox and subsequently amplified via a piezo amplifier module (E-503.00, Physik Instrumente) with a fixed gain of 10 to provide excitation voltage (0~100 V). The output displacement of each axis is within 0~100 μm, which can be read through a PZT servo submodule (E-509.C3A, Physik Instrumente) and is passed to the data input module in dSPACE MicroLabBox.

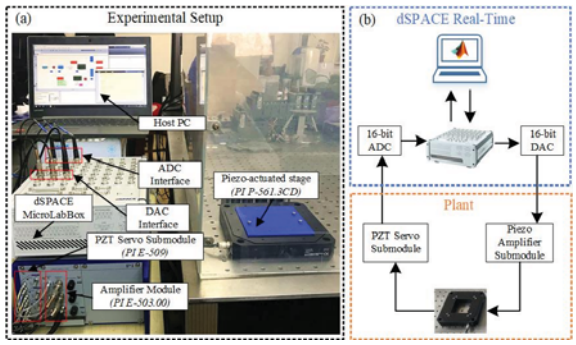

Figure 1. Experimental setup of the piezo nanopositioning platform (a) Experimental hardware (b) Signal flow and software environment

In this work, only the *x*- and *y*-axis were used to implement the proposed control framework for the identified TITO systems and the sampling frequency was set as 10 kHz.

B. System Identification

A linear model of the dominating and cross coupling dynamics in the *xy*-plane is identified by applying a step voltage at 10 V into *x*-axis and *y*-axis alternately. As shown in (1), x_1 [μm] and y_1 [μm] are the corresponding outputs of *x*-axis input u_x [V], while x_2 [μm] and y_2 [μm] are produced by u_y [V].

$$G_{TITO}(s)=\begin{bmatrix} G_{xx}(s) & G_{yx}(s) \\ G_{xy}(s) & G_{yy}(s) \end{bmatrix}=\begin{bmatrix} x_1(s)/u_x(s) & x_2(s)/u_y(s) \\ y_1(s)/u_x(s) & y_2(s)/u_y(s) \end{bmatrix}$$

$$=\begin{bmatrix} \dfrac{1.186\times10^{6}}{s^2+120.5s+1.698\times10^{6}} & \dfrac{\begin{array}{l}7.884s^4-1.302\times10^{4}s^3\\+1.833\times10^{7}s^2-2.009\times10^{10}s\\-1.313\times10^{12}\end{array}}{\begin{array}{l}s^5+411.4s^4+3.375\times10^{6}s^3\\+1.0955\times10^{9}s^2+2.842\times10^{12}\end{array}} \\ \dfrac{\begin{array}{l}7.884s^4-1.302\times10^{4}s^3\\+1.833\times10^{7}s^2-2.009\times10^{10}s\\-1.313\times10^{12}\end{array}}{\begin{array}{l}s^5+411.4s^4+3.375\times10^{6}s^3\\+1.0955\times10^{9}s^2+2.842\times10^{12}\end{array}} & \dfrac{1.154\times10^{6}}{s^2+120.5s+1.698\times10^{6}} \end{bmatrix} \quad (1)$$

The bode diagram of the identified TITO system is presented in Fig. 2. It can be seen that in the dominating directions, the system is lightly damped around 207 Hz with a magnitude more than 17 dB. For the cross coupling directions, the system is well decoupled below 100 Hz, but the lightly damped effect turns to be strong (> 3 dB) around the first resonance, that is the reason why decoupling still need for the already decoupled mechanical design in low frequency.

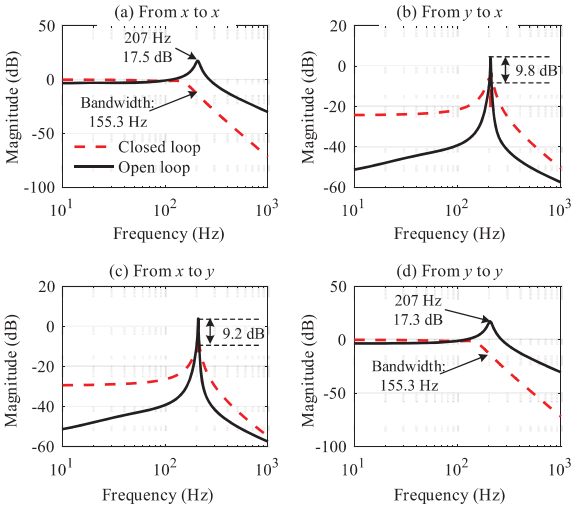

Figure 2. Bode diagram of the identified open loop and the closed loop with static decoupling matrix and IRC control

III. Static Decoupling Matrix Design

As stated before, decoupling around the first resonance needs to be designed. Inspired by the work in [18], the reference model matching approach is adopted for high frequency decoupling of the identified TITO system.

The static decoupling matrix is designed to attenuate the cross coupling effect around the first resonance while

maintain the dynamics in the dominating directions. The transfer function of the desired closed-loop TITO system is,

$$T(s)=\frac{1}{\frac{1}{\omega_b}s+1}\begin{bmatrix}1 & 0\\ 0 & 1\end{bmatrix} \tag{2}$$

where, ω_b is the desired closed-loop bandwidth. The first resonance of both the two axes occurs at 207 Hz. If the bandwidth is set as $\omega_b > 207Hz$, the control input will be large for that the original open loop system rolls off quickly after the first resonance, which may lead to controller saturation. Herein, the desired closed-loop bandwidth is set as $\omega_b = 207Hz$. Then, the static decoupling matrix $\Lambda_{2\times2}$ can be obtained by minimizing the following objective function as

$$\left\|E(s)\right\|_\infty = \left\|G_{TITO}(s)\cdot\Lambda_{2\times2}-T(s)\right\|_\infty \tag{3}$$

Applying the *'fmincon'* command in MATLAB Optimization Toolbox, and set the initial value and the range as,

$$(\Lambda_{2\times2})_0=\begin{bmatrix}1 & 0\\ 0 & 1\end{bmatrix} \tag{4}$$

$$\begin{bmatrix}0.5 & -0.5\\ -0.5 & 0.5\end{bmatrix}\le\Lambda_{2\times2}\le\begin{bmatrix}1.5 & 0.5\\ 0.5 & 1.5\end{bmatrix} \tag{5}$$

The searched result is,

$$\Lambda_{2\times2}=\begin{bmatrix}0.5276 & -0.0482\\ -0.0868 & 0.5262\end{bmatrix} \tag{6}$$

The contrastive frequency responses are described in Fig. 2. From the non-leading diagonal diagrams, the cross coupling effect around the first resonance is relieved from more than 3 dB to less than -5 dB. An extreme case is simulated to evaluate the performance of decoupling matrix by inputting 207 Hz sinusoid signals into *x*-axis and recording the cross coupling outputs of *y*-axis. Results are shown in Fig. 3. It is found that the cross coupling effect is improved by 75% after adding static decoupling matrix.

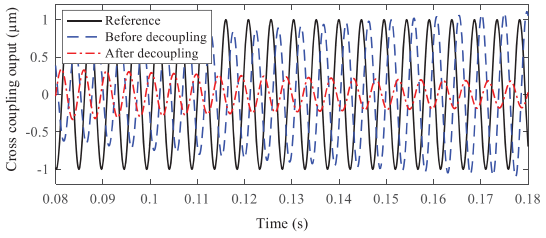

Figure 3. Cross coupling outputs before/after adding static decoupling matrix

It should be noted that, the optimization processes using reference model matching approach in [18] and in this work are different. To be specific, this optimization step in [18] is followed by two single-input-single-output (SISO) controllers' design for each axis, therefore the matrix as well as the controller gains are searched together for achieving the desired TITO closed-loop, which leads to a complex optimization process with 13 parameters. While, in this work, we propose to design the decoupling matrix first, i.e., only the four parameters in the matrix need to be searched in the optimization process, which simplifies the overall design.

IV. Integrated IRC and ILC Design

The identified TITO system is decoupled through adding a static decoupling matrix. After this, the feedback IRC controller to damp each axis can be designed by regarding the dominating dynamics as two SISO systems. Then, a TITO ILC controller can be integrated with the damped system. The integrated framework as well as the convergence analysis will be the main work in this section.

A. Standard IRC

The standard IRC approach was first proposed in the work of [28], and then an analytical approach for the parameters' design was discussed in [29]. It has been proved effective and efficient in vibration attenuation for lightly damped systems like piezo-actuated nanopositioners. Only two integral and a feedthrough term are utilized in this controller, which makes it easy for implementation.

Considering a second-order system with the transfer function as,

$$G(s)=\frac{\sigma^2}{s^2+2\xi_n\omega_n\cdot s+\omega_n^2} \tag{7}$$

where, σ^2 is the mode gain, ξ_n denotes the natural coefficient and ω_n is the natural frequency. For a lightly damped system, $\xi_n \ll 1$ for this mode at the resonant frequency of ω_n.

The standard IRC structure is presented in Fig. 4, where the nominal system $G(s)$ is paralleled with a feedthrough term d, and then damped by the integral controller $C_d(s)$. An integral $C_t(s)$ in the outer loop is applied to improve the tracking performance.

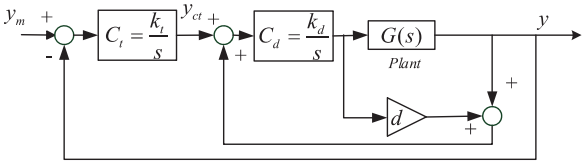

Figure 4. Standard IRC structure

The feedthrough term d is determined as

$$d=-2\cdot\frac{\sigma^2}{\omega_n^2} \tag{8}$$

Then the damping controller gain is chosen to obtain the maximum damping ratio of the inner loop. The achievable maximum damping ratio can be calculated as,

$$\xi_{\max}=\frac{1}{2}\left(\frac{\omega_n}{\sqrt{\omega_n^2+\sigma^2/d}}-1\right) \tag{9}$$

with the corresponding damping controller gain as

$$k_d\,|_{\varepsilon_{\max}} = \frac{1}{|d|}\left(\omega_n \cdot \sqrt{\frac{\omega_n}{\sqrt{\omega_n^2+\sigma^2/d}}}\right) \tag{10}$$

With respect to the tracking controller gain, a trial and error method or a graphics method described in [13] can be used.

B. Integrated IRC and ILC framework

To improve the tracking performance in the repetitive scanning motions of nanopositioners, the ILC can be integrated with standard IRC as shown in Fig. 5. In this framework, the decoupled system through the designed static decoupling matrix is denoted as $\hat{G}_{TITO}(s)$ with

$$\hat{G}_{TITO}(s) = G_{TITO}(s)\cdot\Lambda_{2\times2} \tag{11}$$

The inner damping loop in Fig. 4 is abbreviated as an equivalent controller, which can be given as

$$\bar{C}_{IRC}(s) = \frac{G(s)+(G(s)+d)\cdot C_{IRC}(s)-1}{G(s)\cdot C_{IRC}(s)} \tag{12}$$

The ILC control input is added between the inner damping loop and the outer tracking loop in Fig. 4 so that the damping dynamics remain unchanged while the tracking controller can be adjusted to keep the composite system stable. Therefore, to implement this framework, the standard IRC controller can be designed first to achieve an ideal damping ratio of the vibrational mode. The parameters in ILC and tracking controller gain can be tuned together to guarantee the convergence of the iterative process.

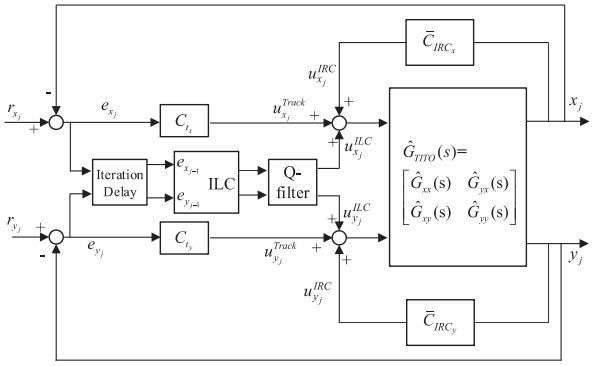

Figure 5. Integrated IRC and ILC framework

C. Monotonic Convergence Condition

A lifted system method which represents the dynamics with matrices in time domain is adopted here to derive the monotonic convergence condition of the composite control system. The details about this method can refer to the survey in [32] and the application in the authors' previous work in [33]. A bold format is utilized in this paper to represent the lifted system.

Take the *x*-axis loop for an instance, the tracking error matrix during the i^{th} iteration in Fig. 5 can be can be computed as,

$$\begin{aligned}\boldsymbol{e}_{x_j} &= \left(\boldsymbol{I}+\boldsymbol{C}_{t_x}\cdot\boldsymbol{L}_{damp_x}\right)^{-1}\cdot\boldsymbol{r}_x - \boldsymbol{L}_{damp_x}\cdot\left(\boldsymbol{I}+\boldsymbol{C}_{t_x}\cdot\boldsymbol{L}_{damp_x}\right)^{-1}\cdot\boldsymbol{u}_{x_j}^{ILC}\\ &= \boldsymbol{S}_x\cdot\boldsymbol{r}_x - \boldsymbol{L}_{damp_x}\cdot\boldsymbol{S}_x\cdot\boldsymbol{u}_{x_j}^{ILC}\end{aligned} \tag{13}$$

where, the damping loop is denoted as,

$$L_{damp_x}(s) = \frac{\hat{G}_{xx}(s)}{1-\hat{G}_{xx}(s)\cdot\bar{C}_{RRC_x}(s)} \tag{14}$$

and $\boldsymbol{S}_x \triangleq \left(\boldsymbol{I}+\boldsymbol{C}_{t_x}\cdot\boldsymbol{L}_{damp_x}\right)^{-1}$ stands for the lifted system matrix of the sensitivity loop of the feedback system.

Applying the proportional-integral-derivative (PID) type learning function, the control output of ILC can be described using a recursion formula as,

$$\boldsymbol{u}_{x_{j+1}}^{ILC} = \boldsymbol{Q}_x\cdot\left[\boldsymbol{u}_{x_j}^{ILC}+\boldsymbol{L}_x\cdot\boldsymbol{e}_{x_j}\right] \tag{15}$$

where, $\boldsymbol{Q}_x$ is the chosen Q-filter, $\boldsymbol{L}_x$ is the designed learning function. Substituting (13) into (15), the control output of ILC can be rearranged as,

$$\boldsymbol{u}_{x_{j+1}}^{ILC} = \boldsymbol{Q}_x\cdot\left[\left(\boldsymbol{I}-\boldsymbol{L}_x\cdot\boldsymbol{L}_{damp_x}\cdot\boldsymbol{S}_x\right)\boldsymbol{u}_{x_j}^{ILC}+\boldsymbol{L}_x\cdot\boldsymbol{S}_x\cdot\boldsymbol{r}_x\right] \tag{16}$$

According to **Theorem 1** in [32], the asymptotic convergence condition for *x*-axis is,

$$\lambda_i\left(\boldsymbol{Q}_x\cdot\left(\boldsymbol{I}-\boldsymbol{L}_x\cdot\boldsymbol{L}_{damp_x}\cdot\boldsymbol{S}_x\right)\right)<1 \tag{17}$$

where, λ_i is the i^{th} eigenvalue of a matrix, and $i\in[1,N]$ in which N stands for the length of a vector or the dimension of a matrix.

Furthermore, the sufficient condition for monotonic convergence of the TITO control system is given as,

$$\bar{\sigma}(M) \triangleq \bar{\sigma}\begin{pmatrix}\boldsymbol{Q}_x\cdot\left(\boldsymbol{I}-\boldsymbol{L}_x\cdot\boldsymbol{L}_{damp_x}\cdot\boldsymbol{S}_x\right)\\ \boldsymbol{Q}_y\cdot\left(\boldsymbol{I}-\boldsymbol{L}_y\cdot\boldsymbol{L}_{damp_y}\cdot\boldsymbol{S}_y\right)\end{pmatrix}<1 \tag{18}$$

where, $\bar{\sigma}$ is the supremum of the singular values of a matrix. It is a stricter condition than (17). Hereto, the parameters of the composite controller should be carefully selected and tuned to guarantee the monotonic condition in (18).

V. Experiments

In this section, the proposed composite framework is evaluated through an application to the experimental platform in Fig. 1. The controllers are designed first for the decoupled TITO system, and the parameters are tuned to satisfy the convergence condition in (18).

A. Feedback Damping Controller Design

From Fig. 2 and (1), it can be seen that the dominating dynamics of *x*- and *y*-axis have the same denominator and only a little difference in mode gains so that the bode diagrams are almost the same. In the damping controller design, the two axes are regarded the same. The designed results based on (8)~(10) are,

$$d_x = -1.39\,,\ d_y = -1.36 \tag{19}$$

$$C_{d_x} = C_{d_y} = \frac{1115}{s} \tag{20}$$

with the achieved maximum damping ratio of the vibrational mode is 0.274 for each axis. The damped

dominating dynamics of each axis can be found in Fig. 2. The damping effect is obvious and the closed-loop bandwidth is obtained as 155.3 Hz for each axis.

B. *Parameters' Tuning of Tracking Controller and ILC*

The tracking controller gains as well as the parameters in the ILC controller are tuned together so that the monotonic condition is satisfied. The results are presented in Table I. It should be noted that the saturation problem of control input is not considered in this paper. Some existing methods can be found in literatures such as [34].

TABLE I. MONOTONIC CONDITION RESULTS

Reference		Parameters					$\bar{\sigma}(M)<1$?
		k_t	ILC			Q-filter	
			P	I	D		
Raster	20 Hz	30 1	0.3 5	0.0 1	0.0 1	70 Hz	0.9517
	40 Hz	30 1	0.3 5	0.0 1	0.0 1	110 Hz	0.9748
Spiral	20 Hz	30 1	0.3 5	0.0 1	0.0 1	80 Hz	0.9254
	40 Hz	30 1	0.3 5	0.0 1	0.0 1	100 Hz	0.9468

Simulations based on the parameters are performed to check the convergence for the references. Results are shown in Fig. 6, which implies that the designed parameters are suitable for the system. The errors in all the cases converge to be stable within 6 iterations with an improvement large than 90% from the first iteration to the last iteration.

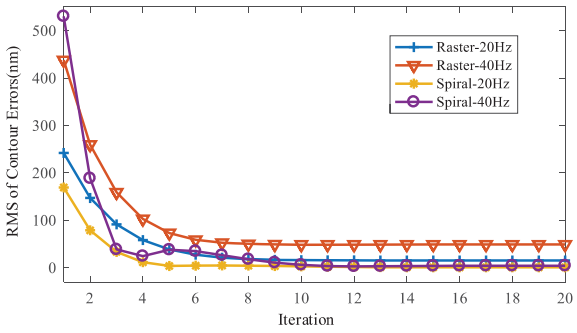

Figure 6. Simulation results of the contour RMS errors during iterations

C. *Tracking Results*

Two typical scanning signals (i.e., raster and spiral) at 20 Hz and 40 Hz were fed into the *x*- and *y*-axis to evaluate the proposed framework's performance.

Raster Scanning: Figure 7 shows the tracking results of the last iteration. Due to the phase lag resulted from the feedback IRC alone, the repetitive errors are evident in each iteration. Through the learning of ILC, these errors are eliminated to a low level as shown in Fig. 7(b) and (d). The RMS errors from the first iteration to the last iteration are reduced by 94% and 85% for 20 Hz and 40 Hz raster signals under IRC + ILC control.

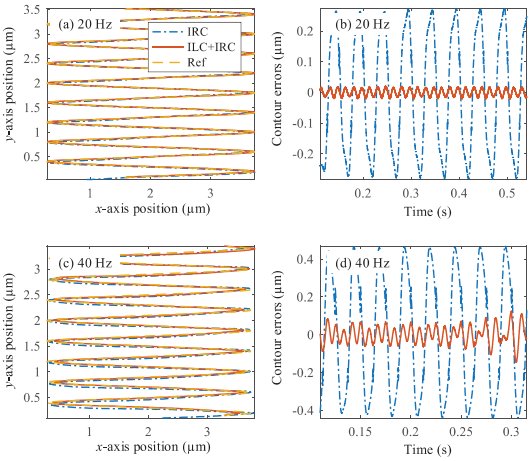

Figure 7. Experimental results of raster scanning in the 20th iteration. (a) *xy*-plane view for 20 Hz. (b) Contour errors comparison for 20 Hz. (c) *xy*-plane view for 40 Hz. (d) Contour errors comparison for 40 Hz.

Spiral Scanning: Results are displayed in Fig. 8, which are consistent with the raster case. To be specific, the RMS errors during the iterative process are cut down by 98% and 96% for 20 Hz and 40 Hz raster signals under IRC + ILC control. This is superior to the raster case, because the frequency components in a spiral are single while those in a raster contain fundamental frequency and harmonic frequencies.

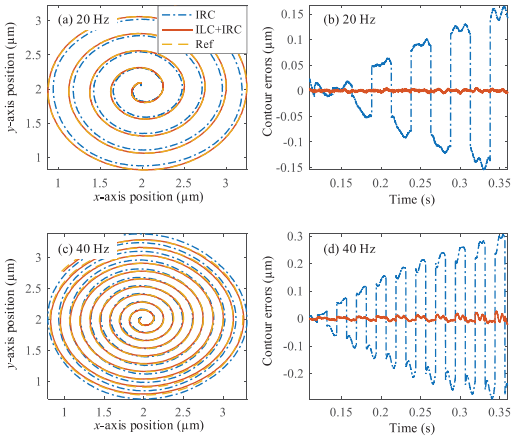

Figure 8. Experimental results of spiral scanning in the 20th iteration. (a) *xy*-plane view for 20 Hz. (b) Contour errors comparison for 20 Hz. (c) *xy*-plane view for 40 Hz. (d) Contour errors comparison for 40 Hz.

VI. CONCLUSION

This paper presents a preliminary try by integrating IRC with ILC for high-speed and high-precision scanning of piezo nanopositioners. For a TITO system, a static decoupling matrix is suggested to relieve the effects caused by cross coupling around first resonance of the system. The lifted system representation is adopted to derive the monotonic convergence condition for the proposed composite control system. Simulation and experimental results demonstrated the effectiveness and superiority of the combination of IRC + ILC compared with IRC alone. Future works will seek to robust IRC and ILC design for load variations of nanopositioners.

REFERENCES

[1] S. K. Das, H. R. Pota, and I. R. Petersen, "A MIMO double resonant controller design for nanopositioners," *IEEE Trans. Nanotechnol*., vol. 14, no. 2, pp. 224-237, Mar. 2015.

[2] Y. K. Yong, S. R. Moheimani, B. J. Kenton, and K. K. Leang, "Invited review article: High-speed flexure-guided nanopositioning: Mechanical design and control issues," *Rev. sci. instrum*., vol. 83, no. 12, pp. 121101, 2012.

[3] Z. Feng, J. Ling, M. Ming, and X. H. Xiao, "High-bandwidth and flexible tracking control for precision motion with application to a piezo nanopositioner," *Rev. Sci. Instrum.*, vol. 88, no. 8, pp. 085107, 2017.

[4] J. Ling, Z. Feng, M. Ming, and X. H. Xiao, "Damping controller design for nanopositioners: A hybrid reference model matching and virtual reference feedback tuning approach," *Int. J. Precis. Eng. Man.*, vol. 19, no. 1, pp. 13-22, 2018.

[5] Z. Feng, J. Ling, M. Ming, and X. H. Xiao, "Data-based double-feedforward controller design for a coupled parallel piezo nanopositioning stage," *Proceedings of the Institution of Mechanical Engineers, Part I: Journal of Systems and Control Engineering*, vol. 231, no. 10, pp. 881-892, 2017.

[6] M. S. Rana, H. R. Pota, and I. R. Petersen, "Nanopositioning performance of MIMO MPC," in *Proc. 10th Asian Control Conference (ASCC)*, Kota Kinabalu, Malaysia, 2015, pp. 1-6.

[7] T. Tuma, A. Sebastian, J. Lygeros, and A. Pantazi, "The four pillars of nanopositioning for scanning probe microscopy: The position sensor, the scanning device, the feedback controller, and the reference trajectory," *IEEE Control Syst.*, vol. 33, no. 6, pp. 68-85, Dec. 2013.

[8] M. Rakotondrabe, "Multivariable classical Prandtl–Ishlinskii hysteresis modeling and compensation and sensorless control of a nonlinear 2-dof piezoactuator," *Nonlinear Dyn.*, vol. 89, no. 1, pp. 481-499, 2017.

[9] A. A. Eielsen, M. Vagia, J. T. Gravdahl, and K. Y. Pettersen, "Damping and tracking control schemes for nanopositioning," *IEEE ASME Trans. Mechatron.*, vol. 19, no. 2, pp. 432-444, Apr. 2014.

[10] Y. K. Yong, K. Liu, and S. O. R. Moheimani, "Reducing cross-coupling in a compliant XY nanopositioner for fast and accurate raster scanning," *IEEE Trans. Control Syst. Technol.*, vol. 18, no. 5, pp. 1172–1179, Sep. 2010.

[11] J. Ling, Z. Feng, M. Ming, and X. H. Xiao, "Combined Model-Free Decoupling Control and Double Resonant Control in Parallel Nanopositioning Stages for Fast and Precise Raster Scanning," In *International Conference on Intelligent Robotics and Applications*, 2016, pp. 51-62.

[12] D. Russell, A. J. Fleming, and S. S. Aphale, "Simultaneous optimization of damping and tracking controller parameters via selective pole placement for enhanced positioning bandwidth of nanopositioners," *ASME J. Dyn. Syst. Meas. Control*, vol. 137, no. 10, pp. 101004, 2015.

[13] C. X. Li, Y. Ding, G. Y. Gu, and L. M. Zhu, "Damping Control of Piezo-Actuated Nanopositioning Stages with Recursive Delayed Position Feedback," *IEEE ASME Trans. Mechatron.*, vol. 22, no. 2, pp. 855-864, Apr. 2017.

[14] Y. Li, and Q. Xu, "Development and assessment of a novel decoupled XY parallel micropositioning platform," *IEEE ASME Trans. Mechatron.*, vol. 15, no. 1, pp. 125-135, Feb. 2010.

[15] Y. Li, and Q. Xu, "Design of a new decoupled XY flexure parallel kinematic manipulator with actuator isolation," in *Proc. IEEE/RSJ Int. Conf. Intell. Robots Syst.,* Nice, France, Sep. 22–26, 2008, pp. 470–475.

[16] M. S. Rana, H. R. Pota, and I. R. Petersen, "Cross-coupling effect compensation of an AFM piezoelectric tube scanner for improved nanopositioning," In *American Control Conference (ACC)*, Portland, OR, USA, 2014, pp. 2456-2461.

[17] S. Bashash, and N. Jalili, "Robust adaptive control of coupled parallel piezo-flexural nanopositioning stages," *IEEE ASME Trans. Mechatron.*, vol. 14, no. 1, pp. 11-20, Feb. 2009.

[18] S. K. Das, H. R. Pota, and I. R. Petersen, "Multivariable negative-imaginary controller design for damping and cross coupling reduction of nanopositioners: a reference model matching approach," *IEEE ASME Trans. Mechatron.*, vol. 20, no. 6, pp. 3123-3134, Dec. 2015.

[19] M. Heertjes, and, A. Van Engelen, "Minimizing cross-talk in high-precision motion systems using data-based dynamic decoupling," *Control Eng. Pract.*, vol. 19, no. 12, pp. 1423-1432, 2011.

[20] A. J. Fleming, and A. G. Wills, "Optimal Periodic Trajectories for Band-Limited Systems," *IEEE Trans. Control Syst. Technol.*, vol. 17, no. 3, pp. 552-562, May 2009.

[21] G. M. Clayton, S. Tien, K. K. Leang, Q. Zou, and S. Devasia, "A review of feedforward control approaches in nanopositioning for high-speed SPM," *ASME J. Dyn. Syst. Meas. Control*, vol. 131, no. 6, pp. 061101, 2009.

[22] K. K. Leang, and S. Devasia, "Design of Hysteresis-Compensating Iterative Learning Control for Piezo-Positioners: Application to Atomic Force Microscopes," *Mechatronics,* vol. 16, no. 3, pp. 141-158, 2006.

[23] Y. Yan, H. Wang, and Q. Zou, "A decoupled inversion-based iterative control approach to multi-axis precision positioning: 3D nanopositioning example," *Automatica*, vol. 48, no. 1, pp. 167-176, 2012.

[24] S. Salapaka, A. Sebastian, J. P. Cleveland, and M. V. Salapaka, "High Bandwidth Nano-Positioner: A Robust Control Approach," *Rev. sci. instrum*., vol. 73, no. 9, pp. 3232-3241, 2002.

[25] S. S. Aphale, A. Ferreira, and S. R. Moheimani, "A Robust Loop-Shaping Approach to Fast and Accurate Nanopositioning," *Sensors Actuat. A-Phys.*, vol. 204, pp. 88-96, 2013.

[26] C. Lee, and S. M. Salapaka, "Fast Robust Nanopositioning – A Linear-Matrix-Inequalities-Based Optimal Control Approach," *IEEE ASME Trans. Mechatron.,* vol. 14, no. 4, pp. 414-422, Aug. 2009.

[27] I. A. Mahmood, and S. O. R. Moheimani, "Making a commercial atomic force microscope more accurate and faster using positive position feedback control," *Rev. sci. instrum*., vol. 80, no. 6, pp. 063705, 2009.

[28] S. S. Aphale, A. J. Fleming, and S. R. Moheimani, "Integral resonant control of collocated smart structures," *Smart. Mater. Struct.*, vol. 16, no. 2, pp. 439–446, 2007.

[29] M. Namavar, A. J. Fleming, M. Aleyaasin, K. Nakkeeran, and S. S. Aphale, "An analytical approach to integral resonant control of second-order systems," *IEEE ASME Trans. Mechatron.*, vol. 19, no. 2, pp. 651-659, 2014.

[30] Kam K. Leang, and S. Devasia, "Feedback-linearized inverse feedforward for creep, hysteresis, and vibration compensation in AFM piezoactuators," *IEEE Trans. Control Syst. Technol.*, vol. 15, no. 5, pp. 927-935, 2007.

[31] E. Brian, H. C. Lee, and A. Douglas, "Combined H∞-feedback control and iterative learning control design with application to nanopositioning systems," *IEEE Trans. Control Syst. Technol.*, vol. 18, no. 2, pp. 336-351, Mar. 2010.

[32] D. A. Bristow, M. Tharayil, and A. G. Alleyne, "A survey of iterative learning control," *IEEE Contr. Syst. Mag.*, vol. 26, no. 3, pp. 96-114, Jun. 2006.

[33] J. Ling, Z. Feng, D. Yao, and X. Xiao, "Non-linear contour tracking using feedback PID and feedforward position domain cross-coupled iterative learning control," *T. I. Meas. Control*, 40(6): 1970-1982, 2018.

[34] N. Sun, Y. Fang, H. Chen, and B. Lu, "Amplitude-saturated nonlinear output feedback antiswing control for underactuated cranes with double-pendulum cargo dynamics," IEEE Trans. Ind. Electron., vol. 64, no. 3, pp. 2135-2146, 2017.